

Largely Improving the Output Performance of Stretchable Triboelectric Nanogenerators via Thermo-Compressive Technology

Qianqian Chen, Aochen Wang, Dan Yang,* Xuelian Wei, Li'ang Zhang, Zhiyi Wu,* Longfei Wang,* and Yong Qin*

Stretchable triboelectric nanogenerators (TENGs) are widely applied in wearable and implantable electronics, smart medical devices, and soft robots. However, it is still a challenge to produce stretchable TENGs with both exceptional elasticity and output performance, which limits their application scope. In this work, high-performance stretchable TENGs are developed through a thermo-compression (TC) fabrication process. In particular, a poly(vinylidene fluoride) film is compactly bound to the elastic thermoplastic polyurethane substrate, which inherits excellent stretchability with a strain of up to 815%. Furthermore, owing to the large surface area, tight contact, and effective vertical transport of tribo-induced charges between the coupled fibrous tribo-layer and soft substrate, the TC composite film-based TENGs exhibit a greater output (2-4 times) than unlaminated film-based TENGs. Additionally, the broad universality of this method is proven using various tribo- and substrate materials. The proposed technology provides a novel and effective approach to conjointly boost the output and stretchability of TENGs, showing encouraging application prospects in self-powered wearable and flexible electronics.

1. Introduction

With the accelerated advance of electronic information technology, multi-functional, highly flexible, and stretchable electronic devices have shown extensive application prospects in various fields such as intelligent medicine,^[1-4] human-machine interaction^[5-7] and artificial intelligence,^[8-9] due to their outstanding characteristics including thinness, softness, and flexibility. Nevertheless, the large-scale manufacturing of flexible electronic products is limited by the complexity of integration and the sustainability of power supply. Since the power supply used in flexible electronic elements is typically a rigid battery, the material and volume constraints impede seamless integration into a flexible system, resulting in the final products with complex structures. At the same time, the inability to avoid repeated charging or replacement has a great


impact on the overall flexibility, lightness, sustainability, and stability of the device. To this end, the development of lightweight, stable, and all-in-one self-powered flexible electronic appliances has become an urgent task. In this regard, TENGs offer an option for the exploitation of self-powered flexible electronics. Based on the coupling of triboelectric and electrostatic effects, TENGs convert irregular mechanical energy from the environment and human body into electrical energy. Flexible and stretchable TENGs are commonly used in biomechanical energy harvesting,^[10-14] self-powered physical health monitoring,^[15-19] and wearable human-machine interaction,^[20-21] serving as competitive energy supply and sensing devices in soft electronics. However, enhancing the output performance of stretchable TENGs to support the increasing growth of flexible electronics toward practical applications is still a challenge.

Many attempts have been made so far to obtain TENGs with high output performance and stretchability. For instance, numerous TENGs have been constructed based on highly flexible polymers such as poly(dimethylsiloxane) (PDMS), acrylic elastomers (e.g., VHB from 3M), and thermoplastic polyurethane (TPU).^[22-31] Reactive ion etching or molding is usually applied to fabricate linear, cubic, or pyramidal micro-nanostructures on the surface of the electrification layer to increase the effective

Q. Chen, L. Zhang, Y. Qin
Institute of Nanoscience and Nanotechnology
School of Materials and Energy
Lanzhou University
Lanzhou 730000, China
E-mail: qinyong@lzu.edu.cn

Q. Chen, A. Wang, X. Wei, L. Zhang, Z. Wu, L. Wang
Beijing Institute of Nanoenergy and Nanosystems
Chinese Academy of Sciences
Beijing 101400, China
E-mail: wuzhiyi@binn.cas.cn; lfwang12@binn.cas.cn

D. Yang
State Key Laboratory of Organic-Inorganic Composites
College of Materials Science and Engineering
Beijing University of Chemical Technology
Beijing 100029, China
E-mail: danyang@buct.edu.cn

 The ORCID identification number(s) for the author(s) of this article can be found under <https://doi.org/10.1002/smll.202307070>

DOI: 10.1002/smll.202307070

working contact area and consequently the triboelectric charge density, thereby improving the output performance of TENGs.^[32] In addition, the surface modification of a stretchable layer or the introduction of other phases into the membrane can effectively enhance the dielectric constant of the triboelectric material and reduce its dielectric loss.^[33–34] Besides the improvement of stretchability, researchers have paid attention to the increase in the output performance of TENGs. Many methods have been proposed to match stretchable triboelectric materials (e.g., silicone rubber), including the design of electrodes with mesh-like, sinuous, and pleated geometries,^[35–37] the dispersion of conductive particles in the elastomer matrix,^[38–40] and the production of intrinsically stretchable conductive materials^[41] and shape-adaptive electrodes (liquid metal or physiological saline^[42–44]). Moreover, TENGs with conductive hydrogels as electrodes demonstrated outstanding stretchability (up to 1000%) while maintaining stable mechanical energy harvesting.^[45–46] Nevertheless, their fatigue susceptibility, weak mechanical toughness, and low electrical conductivity under long-term loading impede their widespread application. Hence, the design of novel device structures and an optimized choice of materials are essential for the exploration of high-output and stretchable TENGs.

Herein, a novel high-output, fully stretchable TC-TENG based on TC composite film consisting of PVDF and TPU (PVDF-TPU TC composite film) was developed. Thanks to the nanostructure and the vertical transport of triboelectric charges, the TC-TENG exhibited impressive output performance with open circuit voltage (V_{oc}) of 230 V and short circuit current (I_{sc}) of 1.5 μ A, which were 18 and 3.8 times greater than those of TPU-TENG (TPU used as the negative electrification layer of TENG) and PVDF-TENG (PVDF electrospun mat used as the negative electrification layer of TENG), respectively. Moreover, the intrinsically high tensile strength of the material in combination with the TC and lamination method endowed the TC-TENG with all-in-one stretchability, preserving the mechanical properties of TPU at almost the initial level (800% elongation at break). In addition, robustness, pressure sensitivity, and general applicability of the TC-TENG were explored as well. The fully stretchable TC-TENG maintained stable output performance without deterioration after 100 cycles in 100% tension stretch-recovery mode. It also exhibited high reliability along with durable signal outputs after 10 000 cycles of the repeated contact-separation motions, as well as high sensitivity to pressure. Therefore, the general applicability of the TC technology was proved, providing new design concepts for upgrading the performance of TENGs and great prospects for their use in wearable electronics, smart displays, and soft robots.

2. Results and Discussion

2.1. Preparation and Characterization of the PVDF-TPU TC Composite Film

Figure 1a depicts the schematic structure of a PVDF-TPU TC composite film, revealing a three-layer laminated structure composed of PVDF nanofibers and elastic TPU. On the top of the TC composite film, the surface PVDF nanofiber mat served as the electrification layer. In the middle part, the electrospun PVDF nanofibers were partly embedded in the TPU film, which en-

sured the integral linkage within the PVDF-TPU TC composite film under stretching. At the bottom, TPU was applied as the supporting and protective layer. The optical photo of the mechanical deformation of the PVDF-TPU TC composite film is shown in **Figure 1b**, confirming that the PVDF-TPU TC composite film not only possessed excellent flexibility through easy roll-up (**Figure 1c**), but also exhibited outstanding stretchability (**Figure 1d,e**). **Figure 1f** displays the preparation process of the PVDF-TPU TC composite film via TC technology. In the obtained PVDF-TPU TC composite film, the bottom part of the nanofiber mat was anchored to the substrate and the top part of the nanofiber mat served as the electrification layer. The properties of the well-matched PVDF-TPU TC composite film depended on the mat thickness, TC temperature (TC-T), and pressure applied. Therefore, the discussion below revolves around the optimizations of these three parameters. 1) Temperature: The electrospun nanofiber mat cannot be embedded in the TPU when the TC-T is less than the thermoplastic softening temperature of TPU (140 °C). In turn, the TPU tends to melt when the temperature is above 200 °C, causing fibers to completely press into the substrate (**Figure S1**, Supporting Information). Finally, the temperature of 170 °C was chosen as the most optimum one. 2) Mat thickness: The impact of thickness is illustrated in **Figure S2** (Supporting Information), according to which the optimum thickness is $\approx 17 \mu$ m (**Figure S2ii**, Supporting Information). A smaller thickness of the mat could lead to poor adhesion, whereas excessive thickness could result in weak surface triboelectric modification. 3) Applied pressure: From a series of experiments (**Figure S3**, Supporting Information), the optimum pressure for the TC process was found to be 25 kPa. The embedded depth of the electrospun mat was closely related to the pressure level. At low pressure, the upper nanofibers were delaminated from the substrate because of the weak junctions between the electrospun mat and TPU after stretching. In contrast, at high pressure, the nanofibers were embedded excessively in the substrate, hence failing to serve as an electrification layer. Therefore, the PVDF-TPU TC composite film was prepared according to the above-optimized parameters.

The SEM images of the surface morphologies of electrospun nanofibers and TPU films are shown in **Figure 1g,h**. The surface of the PVDF-TPU TC composite film after the TC process (depicted in **Figure 1i**) still retained the random nanofiber morphology, which indicated that the film with nanofibrous structure could improve the triboelectric output performance through the increase in contact area. It can be clearly seen from the cross-section morphology in **Figure 1j** that the fibers were well embedded in the TPU layer at the interface, which improved the stretchability of the PVDF-TPU TC composite film.

2.2. Stretchability of the PVDF-TPU TC Composite Film

In order to demonstrate the stretching performance of the PVDF-TPU TC composite film and to observe the state of the fiber mat under stretching, the PVDF-TPU TC composite film was fixed on a flexible electronic test machine and uniaxially stretched at the rates of 100% and 200%, and then eventually recovered its initial state (see **Figure 2a**). The corresponding SEM images of the original, stretched, and recovered PVDF-TPU TC composite film are shown in **Figure 2b**, revealing no obvious

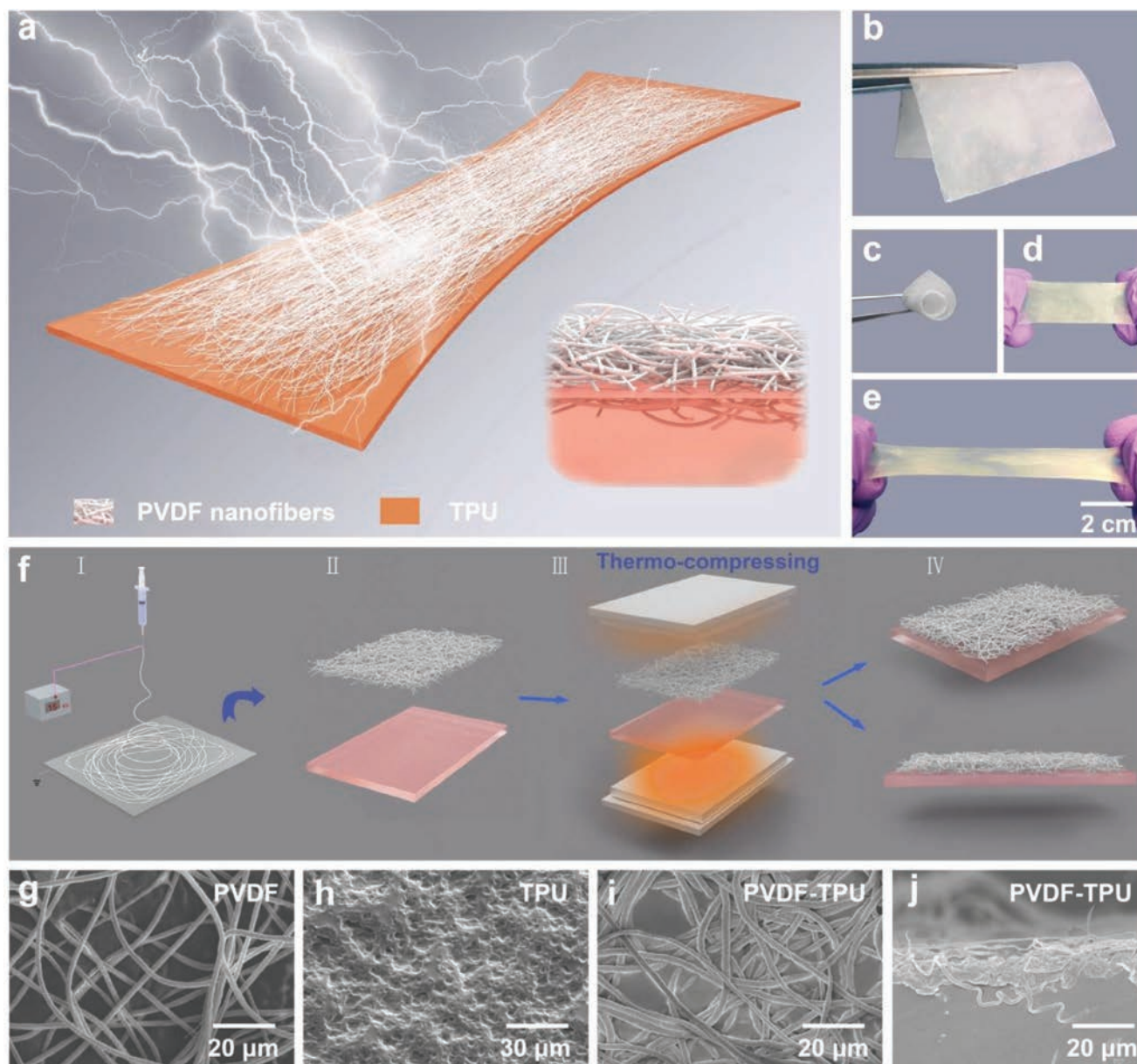


Figure 1. Schematic diagram of the PVDF-TPU TC film and preparation process. a) Schematic diagram of PVDF-TPU TC film (the inset shows the cross-section). b) Optical photograph of the PVDF-TPU TC film. c) Rolled PVDF-TPU TC film showing excellent flexibility. d,e) Digital photograph revealing the stretchability of the PVDF-TPU TC film. f) Schematic diagram of the preparation of the PVDF-TPU TC film via TC technology. g–j) SEM images of g) PVDF electrospun fibers, h) TPU film, i) PVDF-TPU TC composite film surface, and j) PVDF-TPU TC composite film.

ruptures of the nanofibers upon stretching. Moreover, the surface morphology of the stretched PVDF-TPU TC composite film exhibited the directional distribution of the surface fibers, which then disappeared without any fracture once the film returned back to its initial state. As a result, the electrospun nanofiber mat in the PVDF-TPU TC composite film possessed exceptional stretchability and elasticity, which are difficult to achieve in a pure electrospun nanofiber mat. Figure 2c displays the stress–strain curves of three types of films (PVDF nanofiber mat, TPU film, and PVDF-TPU TC composite film). The plot of the PVDF-TPU TC composite film followed a trend almost identical to that of

TPU. Moreover, the tensile strength of the PVDF-TPU TC composite film rose from 0.3 to 37.7 MPa. This behavior was different from the electrospun PVDF nanofiber film (see the inset), which broke when stretched to 18% only. In addition, the elongation at the break of the PVDF-TPU TC composite film increased from 18% to 815%, thereby demonstrating the remarkable stretchability of the specimen. As shown in Figure 2d, the PVDF-TPU TC composite film demonstrated superior tensile repeatability and recovery curve trajectory throughout the stretching cycling test (20 times of cyclic stretching), reflecting an exceptional elastic recovery performance.

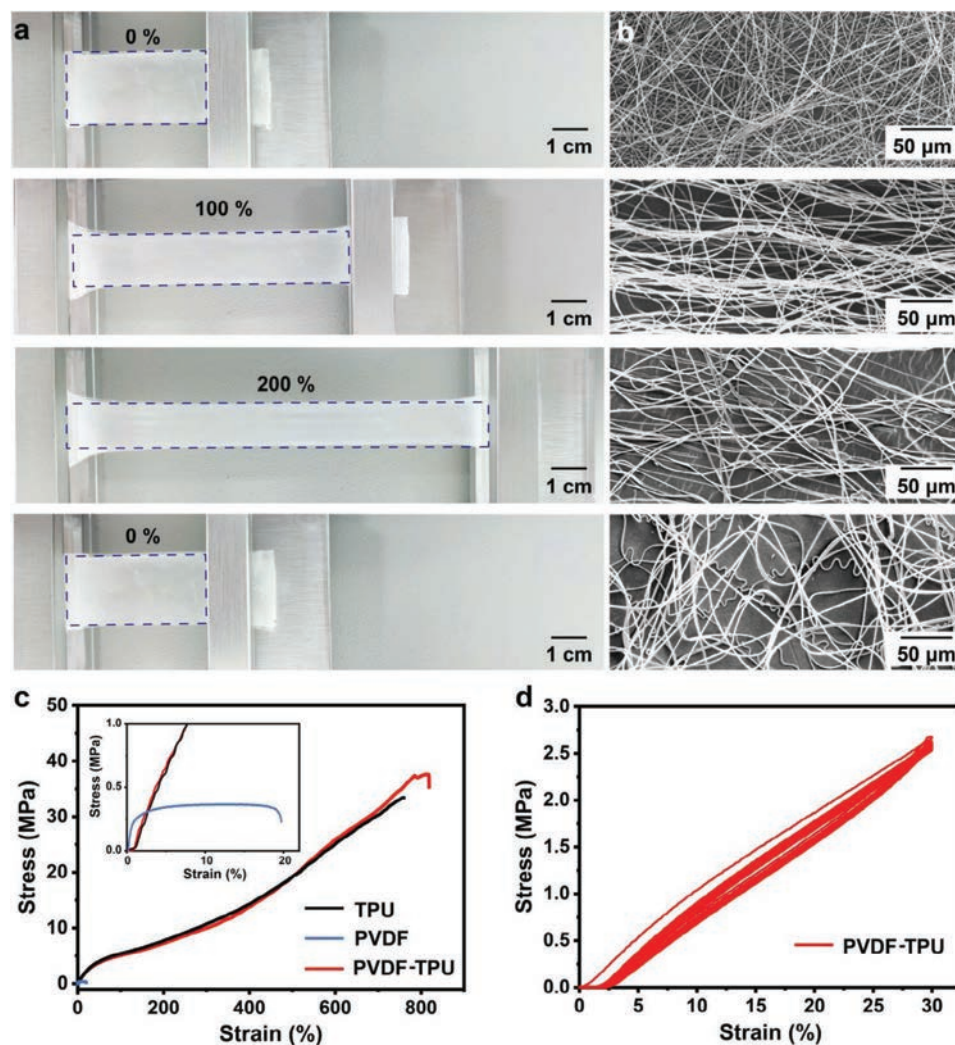


Figure 2. Stretchability characterization of PVDF-TPU TC composite film. a) Optical images in different tensile states (0%, 100%, 200%, back to the initial state). b) SEM images corresponding to the tensile state. c) Stress–strain curves of TPU film, PVDF fiber mat, and PVDF-TPU TC composite film. d) Cyclic tensile test revealing the excellent elastic properties of PVDF-TPU TC composite film.

2.3. Improved Output Performance of TENG Based on PVDF-TPU TC Composite Film

To evaluate whether the output performance of TENG can be improved by the PVDF-TPU TC composite film, three testing films including pure TPU film, electrospun PVDF fiber mat, and PVDF-TPU TC composite film were respectively prepared as the electrification layers to realize the contact-separation mode of TENGs. As shown in **Figure 3a**, the structure of this TENG mainly consisted of two parts. The upper part was composed of the base, Ag nanowires (NWs) electrode, and nitrile rubber (NBR) membrane, serving as the positive electrification layer. The lower part was made of PVDF-TPU TC composite film, Ag NWs electrode, and base, applied as the negative electrification layer. The working principle of the PVDF-TPU TC composite film-based TENG is depicted in **Figure 3b**, in which the contact-separation mode is turned on to detect the triboelectric output performance of different films. A PVDF-TPU-based TENG during the contact-

separation process was used for comparison, wherein the positive charges were generated on the NBR side and the negative charges were generated on the PVDF layer, respectively. During the separation, the Cu electrodes connected with the NBR and the PVDF layer induced the opposite charges according to the inductive effect between the electrodes. A linear motor (see **Figure S4**, Supporting Information) was further employed to realize the periodic pressing-releasing mode, and an electrometer was applied to measure the output triboelectric signals. It was found that the output performance (including open-circuit voltage, short-circuit current, and transferred charges) of the PVDF-TPU TC composite film was much higher than that of the TPU and PVDF film at a driving frequency of 1 Hz (**Figure 3c–e**). The difference in output performance could be explained as follows. First, PVDF has a more negative polarity than TPU.^[47] Second, the nanofiber possesses a relatively large specific surface area. Both these factors contributed to the generation of abundant surface charges during the contact-separation process, thereby

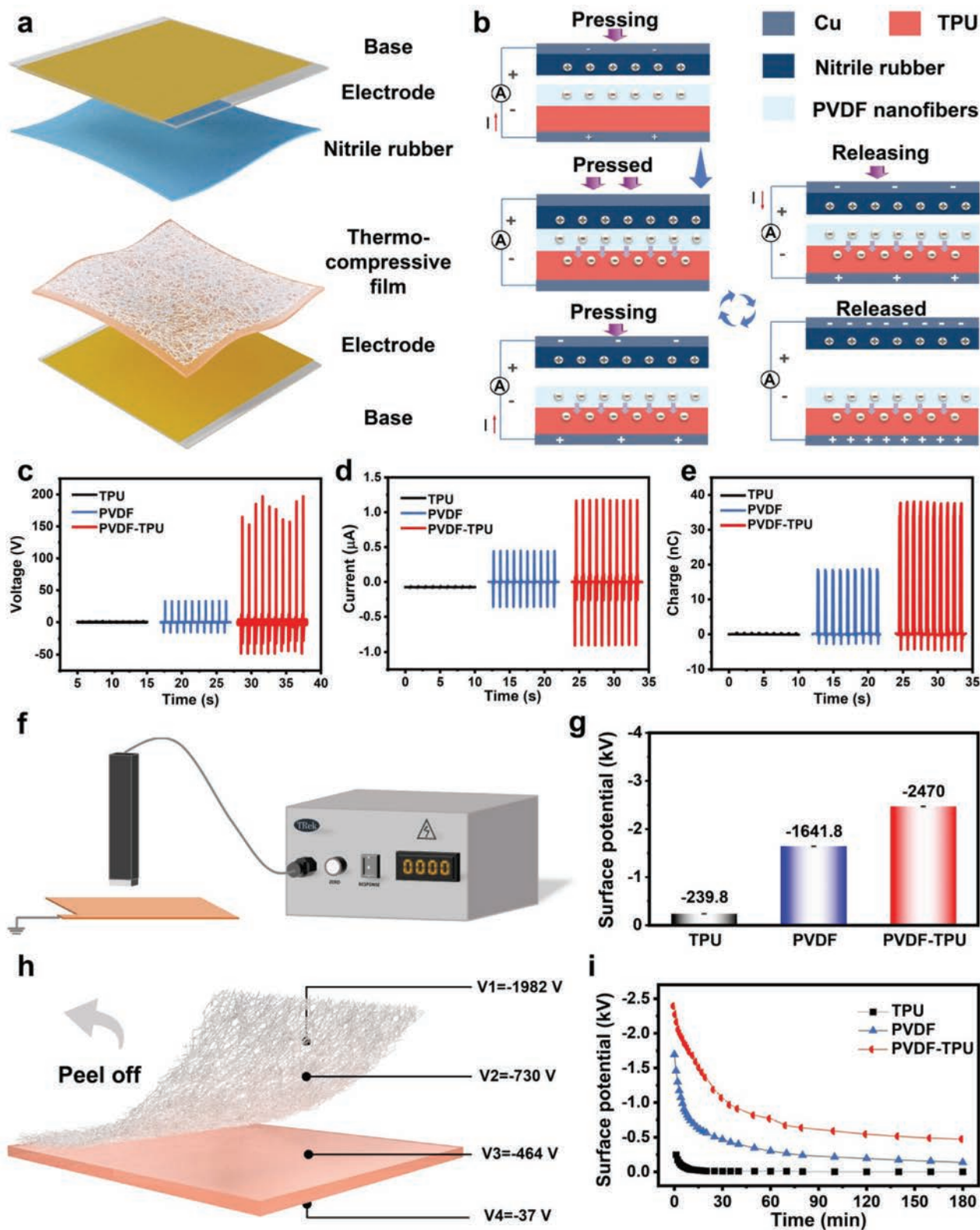


Figure 3. Improving output performance of TENG. a) Schematic diagram of PVDF-TPU TC composite film-based TENG. b) Working principle of PVDF-TPU TC composite film-based TENG. c) Open-circuit voltages, d) short-circuit currents, and e) output charges of TENGs fabricated based on the pure TPU film, electrospun PVDF fiber mat, and PVDF-TPU TC composite film, respectively. f) Diagram of the surface potentials of TPU, PVDF, and PVDF-TPU TC composite film. g) Surface potentials after working. h) Upper and lower surface potentials of the stacked PVDF fiber mat and TPU film without TC, demonstrating the charge transfer process. i) Decay process of the surface potentials of TPU, PVDF, and PVDF-TPU TC composite film.

improving the output performance. More importantly, the output performance of the PVDF-TPU TC composite film-based TENG was also superior to that of the electrospun PVDF nanofiber mat. The reason for this improvement might be the vertical transport of tribo-induced charges. It was assumed that the surface charges tended to diffuse toward the elastic TPU substrate after a period of TENG operation. Since the charges near the contact surface inhibited the generation of new charges, the surface charges diffused deeper and were captured by defects in the polymer, promoting an increase in the contact surface charges and further enhancing the output performance. In order to verify this conjecture, a series of experiments was conducted. In particular, the surface potentials of the three electrification layers were measured over the same working cycles by positioning the surface potentiometer at the same distance from the film surface (Figure 3f). As shown in Figure 3g, the PVDF-TPU TC composite film showed higher surface potential than TPU and electrospun PVDF film, implying that the former composite film had a greater surface charge. To further confirm the feasible flow of charge to the TPU layer with subsequent storage therein, the surface potential relationship was then studied separately from top to bottom of the stacked PVDF mat and TPU film (PVDF/TPU) structure without a thermo-compressive process. As shown in Figure 3h, the top-to-bottom potentials corresponding to different depths of the electrospun PVDF mat and TPU film were -1982 V (0 μm), -730 V (17 μm), -464 V (17 μm), and -37 V (47 μm), respectively. Table S2 (Supporting Information) presents the surface potentials and average values of TPU, PVDF-TPU TC composite film, PVDF/TPU, and PVDF/TPU structures after removing the electrospun mat from the surface of TPU. The results of static triboelectric potential distribution of corresponding TENGs were simulated by COMSOL, as shown in Figure S8 (Supporting Information), which indicated that the composite film possessed a larger potential difference.^[48–50] Finally, the surface potential decay curves of the three membranes were recorded under the same testing conditions. According to Figure 3i, the TPU film showed the fastest decay rate while the PVDF-TPU TC composite film exhibited the slowest potential decay. These results confirmed that there was a tendency for the charge to move toward the TPU film and be stored therein, providing a theoretical basis for the design of stretchable TENGs with high output performance in the future. Considering the excellent triboelectric performance of the PVDF-TPU TC composite film, the following experiments were conducted on the PVDF-TPU TC-based TENG (hereinafter labeled as TC-TENG).

2.4. Output Performance of Fully Stretchable TC-TENG

To obtain fully stretchable TENG devices, the rigid base for the above experiment was replaced with TPU, as shown in Figure 4a. The structure of the fully stretchable TC-TENG is illustrated in Figure 4b. The output performance of the fully stretchable TC-TENG with an effective contact area of 3.5×4 cm^2 was further characterized by periodically displacing a linear motor with a maximum motion distance of 15 mm and a frequency of 1 Hz. As seen from Figure S5 (Supporting Information), the open-circuit voltage, the short-circuit current and the transferred charge were 230 V, 1.5 μA , and 50 nC, respectively. With the

increase in load (Figure 4c), the output voltage became higher, whereas the current decreased. The maximum output power density was 0.28 W m^{-2} at a load of 50 $\text{M}\Omega$ (Figure 4d). Figure 4e depicts the charging capability of the fully stretchable TC-TENG for various capacitors (1 , 2.2 , 3.3 , 4.7 , 10 , and 22 μF), where the charging rate decreased with an increase in capacitance values. In addition, the long-time working stability of the fully stretchable TC-TENG was tested (see Figure 4f). The short-circuit current of the TC-TENG remained stable over $10\,000$ operating cycles. Finally, the energy harvesting ability and applicability of the TC-TENG were assessed. The energy generated by the fully stretchable TC-TENG was sufficient to power 27 green light-emitting diode (LED) lights, as shown in Figure 4g (before lighting) and Figure 4h (after lighting).

Ensuring stable output performance after stretching and recovery is a pivotal feature for stretchable TENGs in practice. According to Figure 4i, the short-circuit current decreased slightly along with elongation during the stretching process. After 100% stretching, the short-circuit current remained at 91.6% of the original state. Furthermore, after returning back to the initial state, the output also recovered its primary value. More importantly, the output of the fully stretchable TC-TENG maintained reliability and stability after 100 cycles of stretching and recovering (see Figure 4j), suggesting a reliable cyclic operation in real applications. Moreover, as shown in Figure 4k, the voltage output of the fully stretchable TC-TENG exhibited a linear increase with an increase in pressure, reaching a sensitivity of 2.01 V kPa^{-1} . Therefore, the above results confirm the application potential of the fully stretchable TC-TENGs for self-powered pressure sensing.

2.5. Universality of TC Technology

According to the above experiments, TC technology is an effective method to significantly improve the output performance of stretchable TENGs. In this regard, a series of investigations was further implemented to verify the applicability of the proposed approach to other electrospun fibers for stretchable TC-TENGs. Several materials including nylon 66 (PA6/6), polyacrylonitrile (PAN), polylactic acid (PLA), polyvinyl chloride (PVC), and cellulose acetate (CA) were also prepared via electrospinning (the spinning parameters are listed in Table S1 (Supporting Information)), and several TC mats were produced by the TC technology, as shown in Figure S6 (Supporting Information). Each TC film was embedded in TENGs, and the output performance of the appliances was tested separately (Figure 5a–c). As expected, the TC film exhibited higher short-circuit current, open-circuit voltage and transferred charge compared to the TPU film and the six electrospun films mentioned above: PA-TPU (0.47 μA , 18 V, 10 nC), PLA-TPU (0.5 μA , 50 V, 10 nC), PAN-TPU (0.7 μA , 54 V, 17.9 nC), PVC-TPU (0.9 μA , 99 V, 21 nC), CA-TPU (1 μA , 81 V, 19.5 nC), and PVDF-TPU (2.1 μA , 180 V, 45 nC). The stress-strain curves (Figure 5d) revealed that the TC film inherited the excellent stretchability of TPU. Based on these findings, it can be concluded that TC technology can greatly improve the output performance of stretchable triboelectric nanogenerators, making it suitable for the preparation of stretchable thin films for self-powered electronic devices.

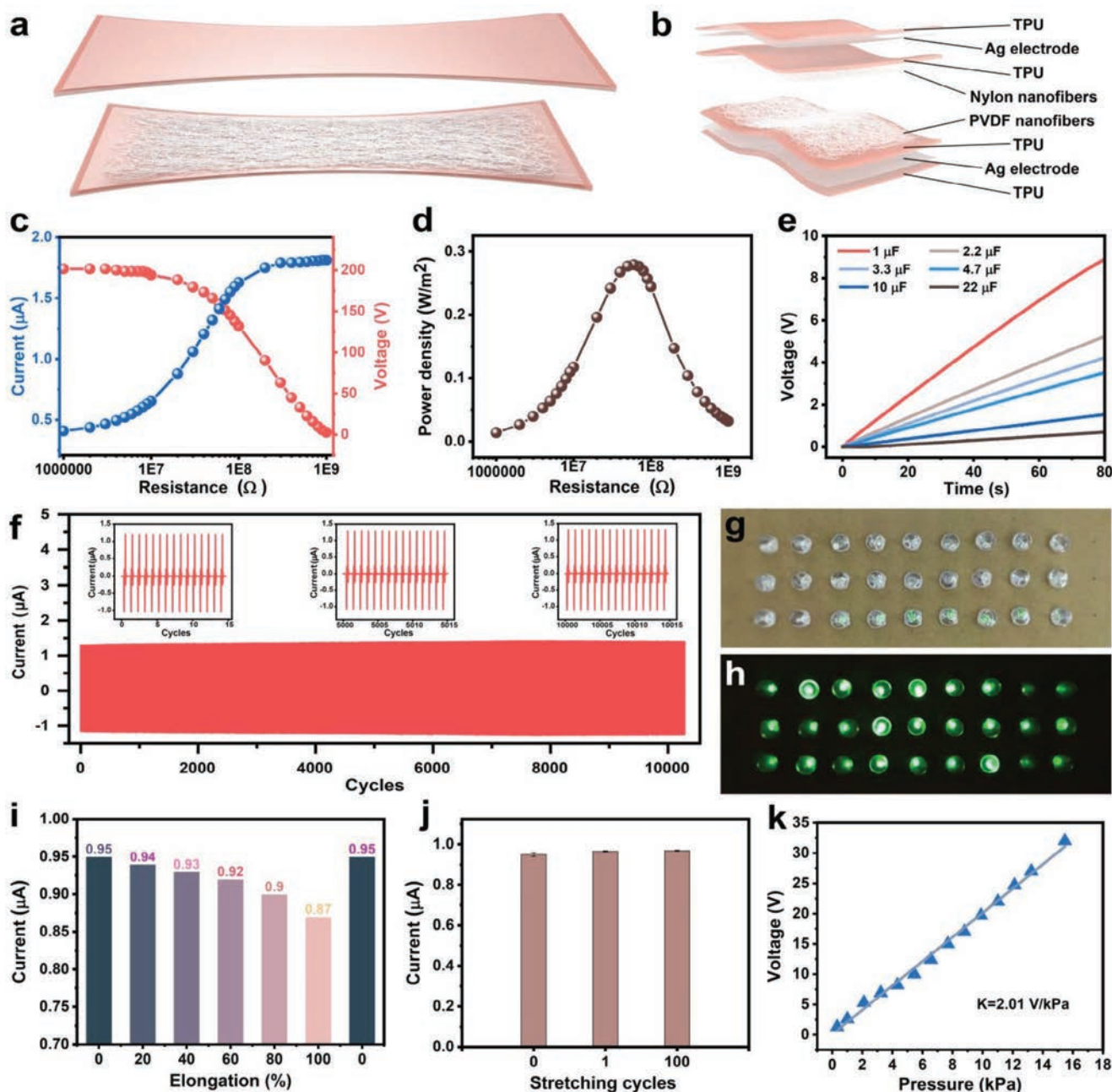


Figure 4. Output performance of the stretchable TC-TENG. a) Schematic diagram of the fully stretchable TC-TENG under an external force. b) Schematic illustration of the structure of the fully stretchable TC-TENG. c) Current and voltage of the fully stretchable TC-TENG under different loads. d) Relationship between power density and load. e) Charging curves of the fully stretchable TC-TENG at various capacities. f) Stability of the fully stretchable TC-TENG during 10 000 working cycles. g, h) Photographs of 27 green LEDs powered by the fully stretchable TC-TENG. i) Output performance of the TC-TENG upon tensile loading and after recovery. j) Output performance of the TC-TENG after 100 cycles of stretching. k) Pressure response of the TC-TENG.

3. Conclusion

In summary, a universal method was proposed to improve the output performance of stretchable TENGs through the lamination of electrospun fiber film with a TPU film by TC technology. The elasticity and stretchability of the PVDF-TPU TC composite film were comparable to those of the TPU film. The 3D network structure of the electrospun fiber mat kept the stretchability of the

PVDF-TPU TC composite film consistent with that of the TPU film, and the elongation at the break of the former film increased by 815%. Moreover, the triboelectric properties of the PVDF-TPU TC composite film were enhanced by 2–4 times compared to the electrospun fiber mat and TPU. The possible reasons were the enhanced effective triboelectric area and the vertical transport of tribo-induced charges, which was confirmed by a series of experiments. In addition, a fully stretchable TC-TENG was

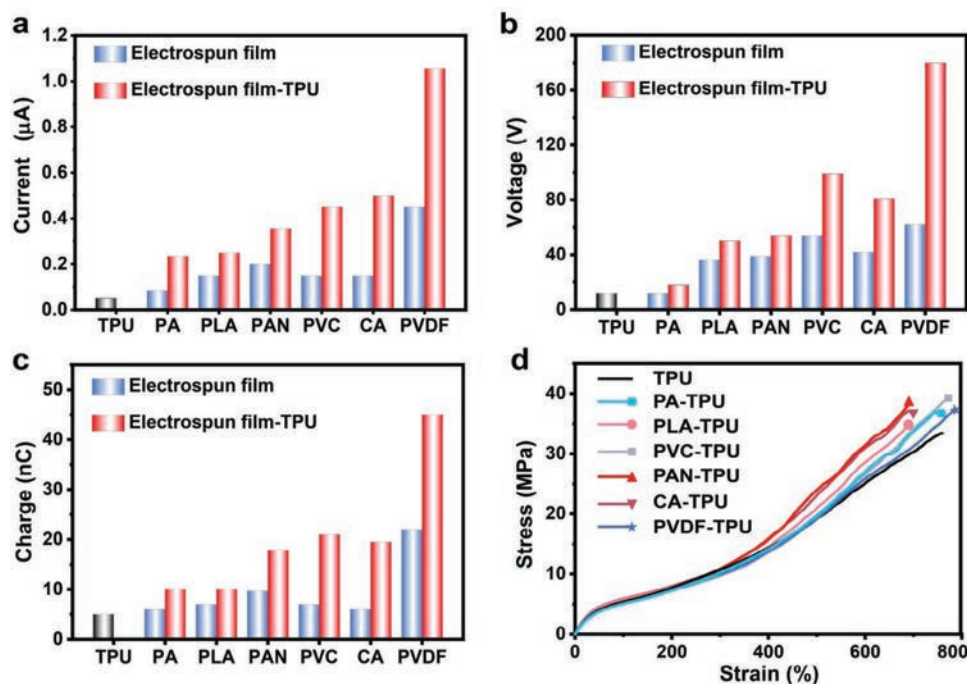


Figure 5. The universality of the method to improve the output of TENGs. The output a) short-circuit current, b) open-circuit voltage, and c) charge quantity of various electrospun fiber films combined with TPU by TC technology, exceeding those of a single electrospun fiber film as the electrification layer of the TENG. d) Stress–strain curves of various electrospun fiber films combined with TPU by TC and a single electrospun fiber film.

developed, which exhibited high output performance. Its open-circuit voltage, short-circuit current, and transferred charge reached the values of 230 V, 1.5 μA , and 50 nC, respectively. The stability and durability of the fully stretchable TC-TENG were demonstrated by long-term working, stretching, and recovering cycling tests (more than 10 000 cycles). Furthermore, the above TC technique is universal for fabricating TC films from electrospun fibers and thermoplastic materials, showing great application potential in energy harvesting and self-powered wearable electronics.

4. Experimental Section

Materials: *N,N*-dimethylacetamide (DMAc, 99%), formic acid (88%), *N,N*-dimethylformamide (DMF, AR, 99.5%), cellulose acetate (CA, acetyl 39.8%, hydroxyl 35%), polylactic acid (PLA, $M_w = 60\ 000$), polyacrylonitrile (PAN, $M_w = 50\ 000$), polyvinyl chloride (PVC, K-value 59-55), and dichloromethane (DCM) were purchased from Shanghai Aladdin Biochemical Technology Co., Ltd., China. TPU film was produced by Xintai Plastic Products Co., Ltd., China. Nylon 6/6 ($M_w = 262.35$) and tetrahydrofuran (THF, $\geq 99.5\%$) were purchased from Shanghai Macklin Biochemical Co., Ltd., China. Poly(vinylidene fluoride) (PVDF, $M_w = 10\ 000\ 000$) was provided by Shanghai Acme Biochemical Co., Ltd., China. Acetone (99.5%) was purchased from Xilong Science Co., Ltd., China.

Preparation of PVDF Nanofiber Mat: The precursor solution for electrospinning was prepared by dissolving 0.42 g of PVDF in 2.58 g of a solvent mixture of DMF/acetone (3:2 vol.%) and stirring for 12 h. The as-prepared PVDF solution was then transferred to a plastic syringe with a 20-gauge metal needle. Electrospinning was afterward carried out with the following parameters: collection distance of 5 cm, applied voltage of 12 kV, solution flow rate of 1 mL h^{-1} , ambient temperature of 20–30 $^{\circ}\text{C}$, and humidity of 30–40%. The nanofiber mat was finally collected to the desired thickness and dried in a vacuum oven at 60 $^{\circ}\text{C}$ for 24 h. The electrospinning parameters are given in Table S1 (Supporting Information).

Fabrication of the PVDF-TPU TC Composite Film and the TC-TENG: Electrospun nanofiber mat ($3.5 \times 4\ \text{cm}^2$, 17 μm) and TPU film ($3.5 \times 4\ \text{cm}^2$, 30 μm) were sandwiched by two heated metal plates (170 $^{\circ}\text{C}$) and subjected to pressure (25 kPa) for 10 s. After the TC process was completed, the PVDF-TPU TC composite film was peeled off and cooled at room temperature. To assemble the TC-TENG, a double-sided conductive copper tape (electrode) with copper wires was adhered to the polyethylene glycol terephthalate (PET) substrate to create a protection layer. A PVDF-TPU TC composite film (40 μm , $3.5 \times 4\ \text{cm}^2$) was then attached to the other side of the electrode to obtain a negative electrification layer. Similarly, NBR (30 μm , $3.5 \times 4\ \text{cm}^2$) was used as a positive electrification layer. Finally, the linear motor periodically drove the connection and disconnection between the two electrification layers, which simulated the mechanical energy harvesting by the TC-TENG.

Characterization and Measurements: The surface morphologies of the electrospun nanofibers, TPU film, and PVDF-TPU TC composite film were characterized via field-emission scanning electron microscopy (FE-SEM, Hitachi SU8020). Uniaxial tensile tests were performed on a mechanical tensile tester (MARK-10 ESM303) connected to a PC, and the stress–strain curves were accurately recorded in real-time on a software platform. A non-contact electrostatic voltmeter (Trek MODEL 347) was used to measure the electrical potential on the surface of the electrification layer. The pressure applied to the TENG was tested and calibrated by a pressure sensor (ZHIFU DS2-500N-XD). A PC software platform was used to control the traveling distance of the linear motor and the frequency of the reciprocating cycle. A Keithley 6514 programmable electrometer and a data acquisition card (NI, USB-6356) were employed to acquire the output data (short-circuit current, open-circuit voltage, and transferred charge) of the TENG, which were eventually recorded in real-time using the Labview software.

Supporting Information

Supporting Information is available from the Wiley Online Library or from the author.

Acknowledgements

Q.Q.C. and A.C.W. contributed equally to this work. This research was supported by the National Key R&D Project from the Minister of Science and Technology (2021YFA1201601), and the National Natural Science Foundation of China (Grant Nos. U21A20175 and 52273259).

Conflict of Interest

The authors declare no conflict of interest.

Data Availability Statement

The data that support the findings of this study are available from the corresponding author upon reasonable request.

Keywords

electrospun nanofibers, stretchable, thermo-compressive technology, triboelectric nanogenerators

Received: August 16, 2023

Revised: October 22, 2023

Published online:

- [1] S. Yao, P. Ren, R. Song, Y. Liu, Q. Huang, J. Dong, B. T. O'connor, Y. Zhu, *Adv. Mater.* **2020**, *32*, 1902343.
- [2] Y. Zhang, Y. Fang, J. Li, Q. Zhou, Y. Xiao, K. Zhang, B. Luo, J. Zhou, B. Hu, *ACS Appl. Mater. Interfaces* **2017**, *9*, 37493.
- [3] W. Zhao, D. Zhang, Y. Yang, C. Du, B. Zhang, *J. Mater. Chem. A* **2021**, *9*, 22082.
- [4] Y. Zhao, Z. Li, S. Song, K. Yang, H. Liu, Z. Yang, J. Wang, B. Yang, Q. Lin, *Adv. Funct. Mater.* **2019**, *29*, 1901474.
- [5] W. Heng, S. Solomon, W. Gao, *Adv. Mater.* **2022**, *34*, 2107902.
- [6] L. Wang, W. Liu, Z. Yan, F. Wang, X. Wang, *Adv. Funct. Mater.* **2020**, *31*, 2007221.
- [7] R. Yin, D. Wang, S. Zhao, Z. Lou, G. Shen, *Adv. Funct. Mater.* **2020**, *31*, 2008936.
- [8] T. Li, Y. Li, T. Zhang, *Acc. Chem. Res.* **2019**, *52*, 288.
- [9] M. Wang, Y. Luo, T. Wang, C. Wan, L. Pan, S. Pan, K. He, A. Neo, X. Chen, *Adv. Mater.* **2021**, *33*, 2003014.
- [10] D. Bao, Z. Wen, J. Shi, L. Xie, H. Jiang, J. Jiang, Y. Yang, W. Liao, X. Sun, *J. Mater. Chem. A* **2020**, *8*, 13787.
- [11] K. Dong, Z. Wu, J. Deng, A. C. Wang, H. Zou, C. Chen, D. Hu, B. Gu, B. Sun, Z. L. Wang, *Adv. Mater.* **2018**, *30*, 1804944.
- [12] M. He, W. Du, Y. Feng, S. Li, W. Wang, X. Zhang, A. Yu, L. Wan, J. Zhai, *Nano Energy* **2021**, *86*, 106058.
- [13] S. S. Kwak, H.-J. Yoon, S.-W. Kim, *Adv. Funct. Mater.* **2019**, *29*, 1804533.
- [14] Z. Wang, Z. Liu, G. Zhao, Z. Zhang, X. Zhao, X. Wan, Y. Zhang, Z. L. Wang, L. Li, *ACS Nano* **2022**, *16*, 1661.
- [15] S.-W. Chen, S.-M. Huang, H.-S. Wu, W.-P. Pan, S.-M. Wei, C.-W. Peng, I.-C. Ni, B. T. Murti, M.-L. Tsai, C.-I. Wu, P.-K. Yang, *Adv. Sci.* **2022**, *9*, 2201507.
- [16] Y. Cheng, W. Zhu, X. Lu, C. Wang, *Nano Energy* **2022**, *102*, 107636.
- [17] X. He, H. Zou, Z. Geng, X. Wang, W. Ding, F. Hu, Y. Zi, C. Xu, S. L. Zhang, H. Yu, M. Xu, W. Zhang, C. Lu, Z. L. Wang, *Adv. Funct. Mater.* **2018**, *28*, 1805540.
- [18] M. Wang, J. Zhang, Y. Tang, J. Li, B. Zhang, E. Liang, Y. Mao, X. Wang, *ACS Nano* **2018**, *12*, 6156.
- [19] Q. Yi, X. Pei, P. Das, H. Qin, S. W. Lee, R. Esfandyarpour, *Nano Energy* **2022**, *101*, 107511.
- [20] J. Cao, X. Fu, H. Zhu, Z. Qu, Y. Qi, Z. Zhang, Z. Zhang, G. Cheng, C. Zhang, J. Ding, *Small Methods* **2022**, *6*, 2200588.
- [21] Z. W. Yang, Y. Pang, L. Zhang, C. Lu, J. Chen, T. Zhou, C. Zhang, Z. L. Wang, *ACS Nano* **2016**, *10*, 10912.
- [22] X. He, Y. Zi, H. Guo, H. Zheng, Y. Xi, C. Wu, J. Wang, W. Zhang, C. Lu, Z. L. Wang, *Adv. Funct. Mater.* **2017**, *27*, 1604378.
- [23] Y. Jiang, K. Dong, X. Li, J. An, D. Wu, X. Peng, J. Yi, C. Ning, R. Cheng, P. Yu, Z. L. Wang, *Adv. Funct. Mater.* **2020**, *31*, 2005584.
- [24] Y.-C. Lai, J. Deng, S. Niu, W. Peng, C. Wu, R. Liu, Z. Wen, Z. L. Wang, *Adv. Mater.* **2016**, *28*, 10024.
- [25] Y. Liu, C. Hu, *Nanoscale* **2020**, *12*, 20118.
- [26] X. Pu, M. Liu, X. Chen, J. Sun, C. Du, Y. Zhang, J. Zhai, W. Hu, Z. L. Wang, *Sci. Adv.* **2017**, *3*, 1700015.
- [27] V. Vallem, Y. Sargolzaeiaval, M. Ozturk, Y.-C. Lai, M. D. Dickey, *Adv. Mater.* **2021**, *33*, 2004832.
- [28] L. Xie, X. Chen, Z. Wen, Y. Yang, J. Shi, C. Chen, M. Peng, Y. Liu, X. Sun, *Nano-Micro Lett.* **2019**, *11*, 39.
- [29] F. Yi, L. Lin, S. Niu, P. K. Yang, Z. Wang, J. Chen, Y. Zhou, Y. Zi, J. Wang, Q. Liao, Y. Zhang, Z. L. Wang, *Adv. Funct. Mater.* **2015**, *25*, 3688.
- [30] F. Yi, X. Wang, S. Niu, S. Li, Y. Yin, K. Dai, G. Zhang, L. Lin, Z. Wen, H. Guo, J. Wang, M.-H. Yeh, Y. Zi, Q. Liao, Z. You, Y. Zhang, Z. L. Wang, *Sci. Adv.* **2016**, *2*, e1501624.
- [31] P. Zhang, Y. Chen, Z. H. Guo, W. Guo, X. Pu, Z. L. Wang, *Adv. Funct. Mater.* **2020**, *30*, 1909252.
- [32] F. R. Fan, W. Tang, Z. L. Wang, *Adv. Mater.* **2016**, *28*, 4283.
- [33] J. Jiang, Q. Guan, Y. Liu, X. Sun, Z. Wen, *Adv. Funct. Mater.* **2021**, *31*, 2105380.
- [34] J. Qian, J. He, S. Qian, J. Zhang, X. Niu, X. Fan, C. Wang, X. Hou, J. Mu, W. Geng, X. Chou, *Adv. Funct. Mater.* **2019**, *30*, 1907414.
- [35] D. C. Kim, H. J. Shim, W. Lee, J. H. Koo, D.-H. Kim, *Adv. Mater.* **2020**, *32*, 1902743.
- [36] N. Matsuhisa, X. Chen, Z. Bao, T. Someya, *Chem. Soc. Rev.* **2019**, *48*, 2946.
- [37] J. A. Rogers, T. Someya, Y. Huang, *Science* **2010**, *327*, 1603.
- [38] H. Fang, X. Wang, Q. Li, D. Peng, Q. Yan, C. Pan, *Adv. Energy Mater.* **2016**, *6*, 1600829.
- [39] Z. Qin, Y. Yin, W. Zhang, C. Li, K. Pan, *ACS Appl. Mater. Interfaces* **2019**, *11*, 12452.
- [40] W. Zhang, Q. Liu, S. Chao, R. Liu, X. Cui, Y. Sun, H. Ouyang, Z. Li, *ACS Appl. Mater. Interfaces* **2021**, *13*, 42966.
- [41] J. Shi, X. Chen, G. Li, N. Sun, H. Jiang, D. Bao, L. Xie, M. Peng, Y. Liu, Z. Wen, X. Sun, *Nanoscale* **2019**, *11*, 7513.
- [42] K. Parida, G. Thangavel, G. Cai, X. Zhou, S. Park, J. Xiong, P. S. Lee, *Nat. Commun.* **2019**, *10*, 2158.
- [43] Y. Yang, J. Han, J. Huang, J. Sun, Z. L. Wang, S. Seo, Q. Sun, *Adv. Funct. Mater.* **2020**, *30*, 1909652.
- [44] Y. Yang, N. Sun, Z. Wen, P. Cheng, H. Zheng, H. Shao, Y. Xia, C. Chen, H. Lan, X. Xie, C. Zhou, J. Zhong, X. Sun, S.-T. Lee, *ACS Nano* **2018**, *12*, 2027.
- [45] L. Dong, M. Wang, J. Wu, C. Zhu, J. Shi, H. Morikawa, *ACS Appl. Mater. Interfaces* **2022**, *14*, 9126.
- [46] X. Jing, H. Li, H.-Y. Mi, P.-Y. Feng, X. Tao, Y. Liu, C. Liu, C. Shen, *ACS Appl. Mater. Interfaces* **2020**, *12*, 23474.
- [47] S. S. H. Abir, M. U. K. Sadaf, S. K. Saha, A. Touhami, K. Lozano, M. J. Uddin, *ACS Appl. Mater. Interfaces* **2021**, *13*, 60401.
- [48] J. Chang, X. He, Z. Yang, X. Bai, C. Yuan, *Nano Energy* **2022**, *167*, 106827.
- [49] Y. Xie, T. Shan, R. Chen, M. Zhang, S. Sun, X. Jian, H.-Y. Mi, C. Liu, C. Shen, *Nano Energy* **2023**, *116*, 108786.
- [50] Y. Xie, Z. Wang, X. Ren, M. F. Antwi-Afari, Y. Wang, H.-Y. Mi, B. Yang, C. Liu, C. Shen, *Compos. Sci. Technol.* **2023**, *237*, 110014.